Article

Evaluation of Aging Resistance of Graphene Oxide Modified Asphalt

Shaopeng Wu, Zhijie Zhao, Yuanyuan Li *, Ling Pang *, Serji Amirkhanian and Martin Riara

State Key Laboratory of Silicate Materials for Architectures, Wuhan University of Technology, Wuhan 430070, China; wusp@whut.edu.cn (S.W.); zzjcbms@126.com (Z.Z.); samirkhanian@eng.ua.edu (S.A.); mriara@seku.ac.ke (M.R.)

* Correspondence: liyuanyuan_09@126.com (Y.L.); lingpang@whut.edu.cn (L.P.);
   Tel.: +86-27-8716-2595 (Y.L. & L.P.)

Abstract: Graphene oxide (GO) has a unique layered structure with excellent gas and liquid blocking properties. It is widely used in many areas, such as gas sensors, carbon-based electronics, impermeable membranes, and polymeric composite materials. In order to evaluate whether GO (1% and 3% by weight of asphalt) can improve the aging resistance performance of the asphalt, 80/100 penetration grade asphalt (90 A) and styrene–butadiene–styrene modified asphalt (SBS MA) were used to prepare the GO modified asphalt by the melt blending method. The surface morphology of the GO was analyzed by scanning electron microscope (SEM). The UV aging test was conducted to simulate the aging during the service period. After UV aging test, the physical performances of GO-modified asphalts were tested, and the $I_{C=O}$ and $I_{S=O}$ increments were tested by Fourier transform infrared spectroscopy (FTIR) to evaluate the aging resistance performance of the GO modified asphalt. In addition, the rheological properties of GO modified asphalts were studied using a dynamic shear rheometer (DSR). The SEM analysis indicated that the GO exhibits many shared edges, and no agglomeration phenomenon was found. With respect to the physical performance test, the FTIR and the DSR results show that GO can improve the UV aging resistance performance of 90 A and SBS MA. In addition, the analysis indicated that the improvement effect of 3% GO is better than the 1% GO. The testing on the rheological properties of the modified asphalt indicated that the GO can also improve the thermo-oxidative aging resistance performance of asphalt.

Keywords: GO modified asphalt; aging resistance; chemical structure; physical performance; rheological property

1. Introduction

Asphalt concrete is widely used as the pavement of choice in many countries. However, asphalt binder will be aged by many factors, such as heat, light, and oxygen during the high-temperature production and natural environment during service. Aging makes the asphalt binder become harder, leads to early damage, and reduces the service life span of the pavement [1,2]. Therefore, to prolong the service life span of an asphalt pavement, it is important to improve the anti-aging performance of the asphalt.

Asphalt aging is mainly caused by oxidation [3]. After aging, the asphalt molecular weight will be increased or associated irreversibly to form macromolecules by absorbing oxygen, the asphalt colloid structure will, therefore, be changed, decreasing the asphalt pavement performance [4,5]. Oxygen not only reacts with the surface asphalt, generates hydroxyl- and the oxygen-containing groups, but also continues aging the interior asphalt by gradually diffusing into the internal asphalt. The main difference of the thermo-oxidative aging and optical oxygen aging is the different excitation source

to generate the free radicals in the initial stage. The excitation sources are the thermal and light excitations [6,7]. There are many possible ways in preventing the asphalt from being aged or in reducing the rate of asphalt aging. Some of these techniques include the following: (a) by reducing the excitation energy (thermal energy or light energy); (b) by reducing the formation rate or concentration of the initial free radicals; or (c) by preventing contact of oxygen with the asphalt, which can reduce the reactant concentration (O_2) of the oxidation reaction in the aging process.

Inorganic nano-materials, such as layered double hydroxides (LDHs) [8], montmorillonite [9,10], and carbon black [11,12], have a layered structure and are excellent barriers for oxygen, which can be used in improving the anti-aging performance of asphalt. However, the compatibility between inorganic materials and organic asphalt is poor, making it difficult for inorganic materials to disperse well in the asphalt; because of the van der Waals forces or the electrostatic forces, they tend to aggregation easily [13]. These drawbacks decrease the barrier performances and reduce the modification effects of the modifiers. Graphene oxide (GO) is a type of layered inorganic nano-material with a molecular structure roughly the same as that of grapheme. GO shows excellent performance in gas and liquid blocking, which is similar to that of graphene [14,15]. The difference of GO compared with graphene is that there are many active oxygen-containing functional groups on the layers and the lamella edges of the GO, which endows GO with good compatibility toward inorganic and organic materials, and makes the graphene oxide-modified material have a low permeability of gas and liquid [16]. In another word, GO not only has the unique layer nanostructures with excellent oxygen barrier performance, but also has good compatibility with the asphalt. Therefore, it is important to conduct more research in this area to determine the effect of GO on the properties of virgin and modified binders.

In order to evaluate to effects of GO on the anti-UV aging performance of the asphalt, two types of asphalt and two levels of the GO contents (1% and 3% by weight of the binder) were utilized in preparing the GO-modified asphalt by the melt-blending method. First, the asphalts were aged by a thin film oven test (TFOT), and then aged by UV aging. After aging, the physical performance tests were conducted to study the performance attenuation during the aging process and the characteristic functional groups were analyzed by Fourier transform infrared spectroscopy (FTIR). The rheological properties were evaluated with a dynamic shear rheometer (DSR) in the temperature range from −10 to 30 °C.

2. Materials and Methods

2.1. Materials

2.1.1. Asphalt

Two types of asphalt binders were used in this research project, namely base asphalt with 80/100 penetration grade (simply referred to as 90 A) and SBS-modified asphalt (simply referred to as SBS MA). They were obtained from Inner Mongolia Xindalu Asphalt Co., Ltd. (Chifeng, Inner Mongolia, China). Technical information of these two asphalt binders are shown in Table 1.

Table 1. Properties of 90 A and SBS MA.

Asphalt	Technical Parameters	Unit	Test Results	Method
90 A	25 °C Penetration	0.1 mm	84.6	ASTM D5 [17]
	Softening point	°C	47.8	ASTM D36 [18]
	10 °C ductility	cm	>100	ASTM D113 [19]
	60 °C viscosity	Pa·s	206	ASTM D4402 [20]
SBS MA	25 °C Penetration	0.1 mm	62.3	ASTM D5 [17]
	Softening point	°C	57.5	ASTM D36 [18]
	5 °C ductility	cm	55.8	ASTM D113 [19]
	135 °C viscosity	Pa·s	1.337	ASTM D4402 [20]

2.1.2. Graphene Oxide

GO was applied to be an anti-aging modifier for the asphalt binders. The GO with 5–10 layers was provided by the Suzhou Heng Ball Graphene Technology Co., Ltd. (Suzhou, China). The purity of GO was higher than 95%, the specific surface area of GO was about 100–300 m^2/g, and the lamella diameter of the GO was about 10–50 um.

2.2. Preparation of GO Modified Asphalt

First, 90 A and SBS MA were heated to 155 °C and 170 °C, respectively; then the design contents of the GO (1.0 wt % or 3.0 wt %) were added to the asphalt binder by using a high-speed shear mixing machine (4000 r/min) for 30 min. Since the heating and shearing of the preparation process inevitably causes the aging of asphalt, and it is rational to evaluate the aging resistance performance of GO-modified asphalt binders at the same condition, the 90 A (and SBS MA) was also exposed to the same heating and shearing process as the GO-modified 90 A (and GO-modified SBS MA).

2.3. Microstructure of GO

The surface morphology of the GO was analyzed by the JSM-5610LV SEM (Tokyo, Japan), the SEM resolution was 3 nm in a high vacuum. The SEM pictures were taken on the microscope at the voltage of 5 KV where the magnification of the pictures could be obtained from 18–300,000 times. The GO, in general, would be affected by thermal shock for its structural metastability [21], so the GO samples were dried at 50 °C.

2.4. Evaluation of Anti-Aging Performance

2.4.1. Aging Procedures

The samples used for the ultraviolet aging were first aged by TFOT (Cangzhou, Hebei, China). The mass of TFOT-aged samples were 50 ± 0.5 g, the diameter of the sample plate was 140 mm, the asphalt film thickness was approximately 3.2 mm, and the test temperature was stable at 163 ± 0.5 °C for 5 h. Then, the UV aging simulation test was performed with a straight-pipe high-pressure mercury lamp, the UV radiation intensity was 2000 uw/cm^2, the UV wavelength was 365 nm, and the aging times were set up to three, six, and nine days. The sample mass of UV aging was 20 ± 0.1 g and the test temperature was stable at 50 ± 0.5 °C.

2.4.2. Physical Performance Tests

Physical performances tests, such as penetration, softening point, ductility, and viscosity, were conducted according to the standards ASTM D5 [17], ASTM D36 [18], ASTM D113 [19], and ASTM D4402 [20], respectively. The temperature of the penetration test was 25 °C, and the ductility tests of 90 A and SBS MA were set to be 10 °C and 5 °C, respectively. Three replicate samples were tested for each of the penetration, ductility, and softening point tests, and the average of the three results was taken as the final result.

2.4.3. Characteristic Functional Group Test

A Fourier transform infrared spectroscopy (FTIR) instrument (Columbus, OH, USA) was used to test the characteristic functional group changes of the asphalts after UV aging, the preparation procedures of asphalt samples for FTIR are described briefly: First, the asphalt CS_2 solution with 5 wt % concentration of asphalt was prepared, then two drops of asphalt CS_2 solution were placed on the KBr chip by the glue dropper, so the thin film asphalt sample could be obtained after the CS_2 was fully volatilized. The scan wave number range was from 4000 to 400 cm^{-1}, and scan times were 64 times.

2.4.4. Rheological Property Test

A SmartPave102 dynamic shear rheometer (DSR) (Graz, Austria) was utilized to test the rheological properties of asphalt binders. The test temperature was in the range of -10 to 30 °C, the rotor diameter was 8.0 mm, the sample thickness was 2.0 mm, frequency was set to 10 rad/s, and the strain was 0.05%.

3. Results and Discussion

3.1. Characterization of the GO

GO has multiple layers of structural material with oxygen functional groups on the basal plane and at the edges [22,23]. Most researchers believe that epoxy and hydroxyl groups are on the basal plane, whereas carbonyl and carboxylic acid groups are at the edges [24–27]. These oxygen functional groups allow the GO to be easily and evenly dispersed because they decrease the van der Waals forces of the GO molecules [21]. The microstructure of the GO was studied by SEM, Figure 1a,b are SEM images of the GO magnified 500 and 1000 times, respectively. From Figure 1, the GO particles are mostly independent states and exhibit lots of shared edges, and the high face-to-face interaction stability or the face-to-edge interactions are not observed in the SEM pictures. Therefore, the GO may show a good compatibility with asphalt. On the other hand, these oxygen functional groups cause some defects on its basal plane and decrease its barrier performance [28,29]. Thus, to improve the barrier property, in this paper, multilayered (5–10) GO was selected as the anti-aging modifier for asphalt.
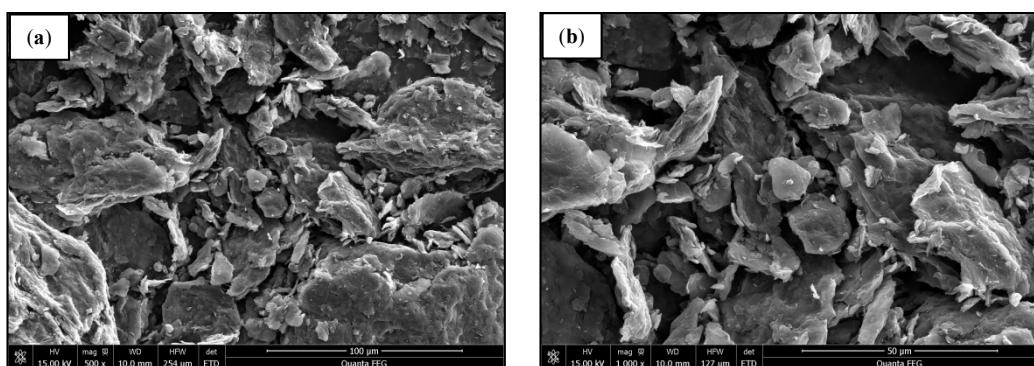
Figure 1. SEM pictures of GO ((**a**) 500×; and (**b**) 1000×).

For its excellent gas-barrier property, GO can also improve the blocking performance of the modified materials to block the gas and the vapor diffusion. The barrier property can extend the travelling pathway of the O_2 when it diffuses to the internal asphalt, and also prolongs the travelling pathway of the volatile organic compounds (VOCs) when released from the asphalt [30–32]. Asphalt aging is mainly caused by oxidation, so the GO may be able to retard the aging of asphalt by decreasing the O_2 diffusion rate.

3.2. UV Aging Resistance Performance

3.2.1. Chemical Structure

The asphalt chemical structure will be changed during the aging process, the characteristic functional groups index, namely carbonyl groups (1700 cm^{-1}) and sulfoxide groups (1032 cm^{-1}), will increase with the increase of aging degree [16,33]. In order to analyze the anti-aging performance of

asphalt, the FTIR was used to test the characteristic functional groups of asphalt binders before and after aging. The $I_{C=O}$ and $I_{S=O}$ were calculated according to the Equations (1) and (2), respectively:

$$I_{C=0} = \frac{S_{1700 \text{ cm}^{-1}}}{S_{2000 \sim 600 \text{ cm}^{-1}}} \tag{1}$$

$$I_{S=0} = \frac{S_{1030 \text{ cm}^{-1}}}{S_{2000 \sim 600 \text{ cm}^{-1}}} \tag{2}$$

where, $S_{1700 \text{ cm}^{-1}}$ expresses the areas of the 1700 cm^{-1} centered carbonyl group absorption band; $S_{1032 \text{ cm}^{-1}}$ expresses the areas of the 1032 cm^{-1} centered sulfoxide group absorption band; $S_{2000 \sim 600 \text{ cm}^{-1}}$ expresses the areas of all absorption bands between 2000 cm^{-1} and 600 cm^{-1}.

The $I_{C=O}$ and $I_{S=O}$ of the aged binders (i.e., TFOT and UV) studied in this research are shown in Figures 2 and 3, respectively. As shown in Figure 2, the $I_{C=O}$ of 90 A and SBS MA were gradually increasing with an increase in the UV aging time, where, 90 A + 1% GO, 90 A + 3% GO, SBS MA + 1% GO, and SBS MA + 3% GO correspond to 90 A with 1% GO, 90 A with 3% GO, SBS MA with 1% GO, and SBS MA with 3% GO, respectively. The results for the $I_{S=O}$ followed a similar trend (Figure 3). After UV aging, the $I_{C=O}$ and $I_{S=O}$ increments of 90 A and SBS MA with GO are smaller than the virgin binder (asphalt without GO), indicating that the GO can improve the UV aging resistance of 90 A and SBS MA, and inhibit the increase in $I_{C=O}$ and $I_{S=O}$ of 90 A and SBS MA during UV aging.
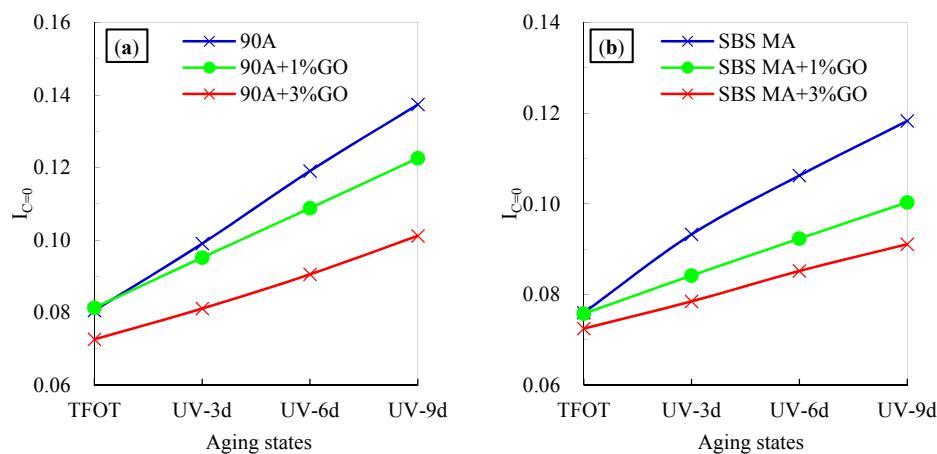
Figure 2. The $I_{C=O}$ of 90 A (**a**) and SBS MA (**b**) after UV aging.
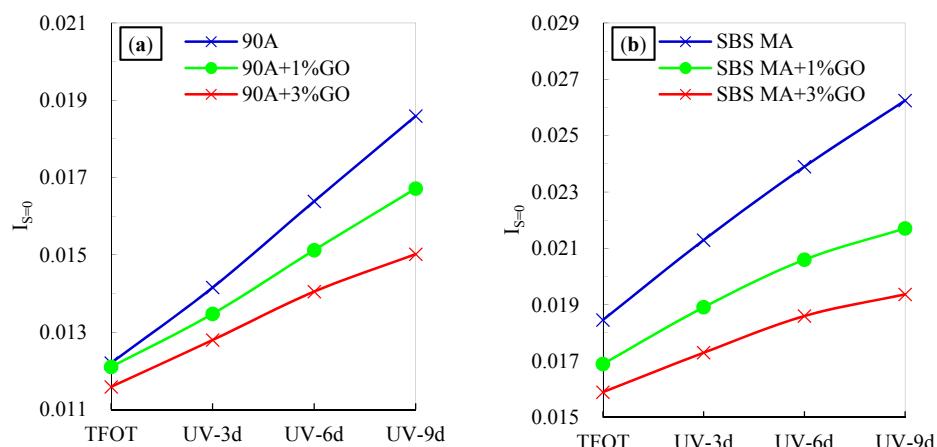
Figure 3. The $I_{S=O}$ of 90 A (**a**) and SBS MA (**b**) after UV aging.

3.2.2. Physical Performance

Three indicators, such as residual penetration ratio (PRR), softening point incremental (SPI), and residual ductility ratio (DRR) can characterize the physical properties attenuation amplitude during the UV aging process. Therefore, these three indicators were used in evaluating the UV aging degree of the asphalts used in this research project. The PRR, the SPI, and the DRR were calculated according to the Equations (3)–(5), respectively:

$$PRR = \frac{P_{UV}}{P_{TFOT}} \times 100\% \tag{3}$$

$$SPI = SP_{UV} - SP_{TFOT} \tag{4}$$

$$DRR = \frac{D_{UV}}{D_{TFOT}} \times 100\% \tag{5}$$

where, P_{TFOT}, D_{TFOT}, and SP_{TFOT} are the penetration (0.1 mm), the ductility (cm), and the softening (°C) after TFOT, respectively; P_{UV}, D_{UV}, and SP_{UV} are the penetration (0.1 mm), the ductility (cm), and the softening (°C) after UV aging, respectively. In general, it is expected that the asphalt with a good UV aging resistance should have higher PRR, lower SPI, and higher DRR values indicating that the physical performance of the asphalt will not change significantly after UV aging.

Figure 4 shows the PRR results after UV aging. It can be seen that the PRR value of all asphalts decrease gradually with the extension of UV aging time, when the UV ageing time increases from three days to nine days, the PRR value of 90 A decreases from 59.2% to 36.4%, and the PRR value of SBS MA decreases from 67.3% to 38.6%. The higher PRR value means a lower aging degree, and vice versa. After adding the GO, the PRR value of 90 A and SBS MA after UV aging increased, when the GO content was 3%, the PRR of 90 A after nine days of UV aging increased from 36.4% to 57.3%. In addition, the PRR value of SBS MA after nine days UV aging increased from 38.6% to 64.3%, which shows that the GO can alleviate asphalt penetration attenuation in the process of UV aging.
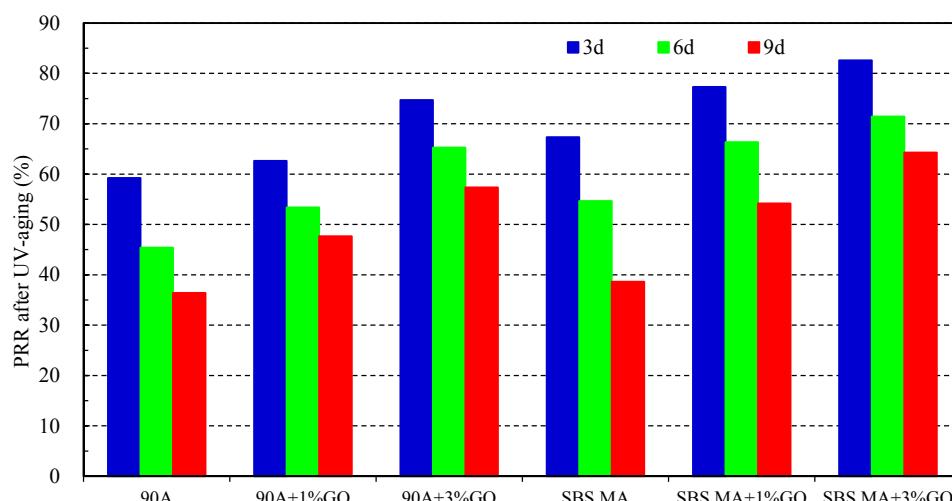
Figure 4. The PRR of asphalt after UV aging.

Figure 5 shows the SPI results after UV aging. The higher the SPI, the higher is the aging degree and vice versa. The SPI values of 90 A, SBS MA and the GO modified asphalts increased gradually with the extension of UV aging time. Compared to the asphalt without modifiers, after adding the GO, the SPI values of all asphalts decreased at the same UV aging condition, and the SPI value was lower when the GO content was 3% compared to 1%. This shows that the GO can retard the softening point increase in the UV irradiation process, and the retarding effect is more pronounced when the GO content is increased.
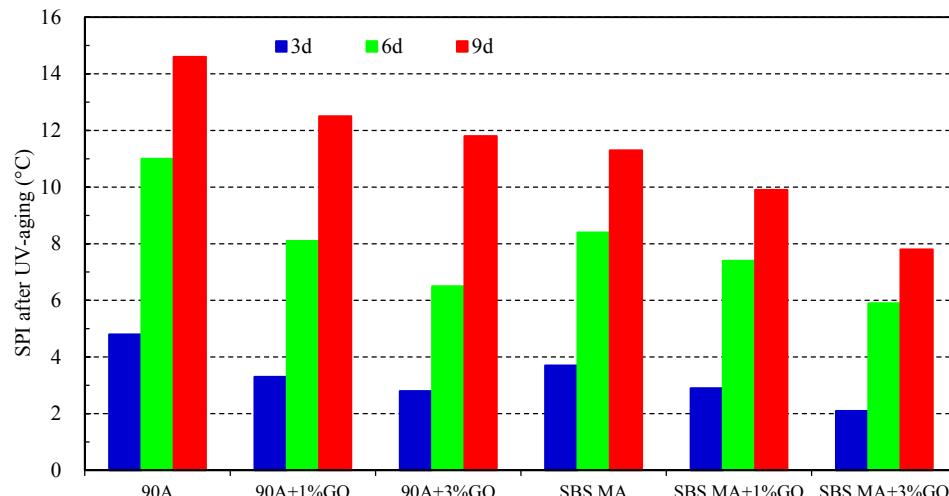
Figure 5. The SPI of asphalt after UV aging.

The DRR results after UV aging are shown in Figure 6. The lower value of DRR indicates an increase in the aging degree of the binder. With the extension of the UV times, the DRR values decrease obviously. At the same UV aging condition, the ductility attenuation rate decreases with the GO, and the decrease effect is more obvious when the GO content is increased from 1% to 3%. For instance, the DRR values of the GO modified 90 A will increase from 21.2% (without GO) to 38.1% (with 3% GO), and the DRR values of the GO modified SBS MA will increase from 25.0% (without GO) to 45.4% (with 3% GO).
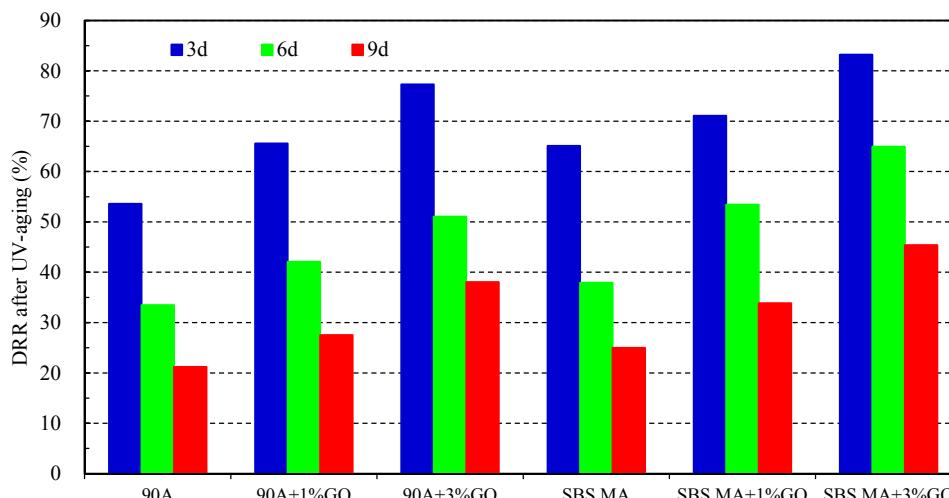
Figure 6. DRR of asphalt after UV aging.

The asphalt viscosity after TFOT and UV aging was tested at different temperatures, namely 30 °C, 45 °C, 60 °C, 75 °C, 90 °C and 105 °C. The viscosity aging indices (VAI) of all temperatures were calculated based on the Equation (6):

$$\text{VAI} = \frac{\text{V}_{\text{UV}} - \text{V}_{\text{TFOT}}}{\text{V}_{\text{TFOT}}} \times 100\% \tag{6}$$

where, V_{UV} is the viscosity after UV aging in Pa·s; and V_{TFOT} is the viscosity after TFOT in Pa·s. In general, a higher VAI value is an indication of a higher UV-aging degree. The VAI results of 90 A

and GO-modified 90 A are shown in Figure 7, and the VAI results of SBS MA and the GO-modified SBS MA are shown in Figure 8.
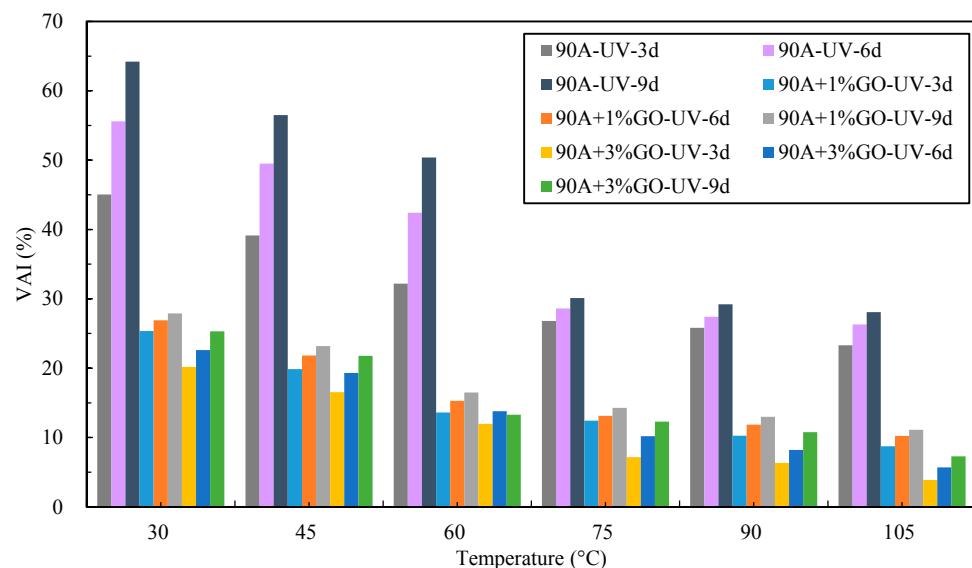
Figure 7. VAI of 90 A and GO modified 90 A after UV aging.
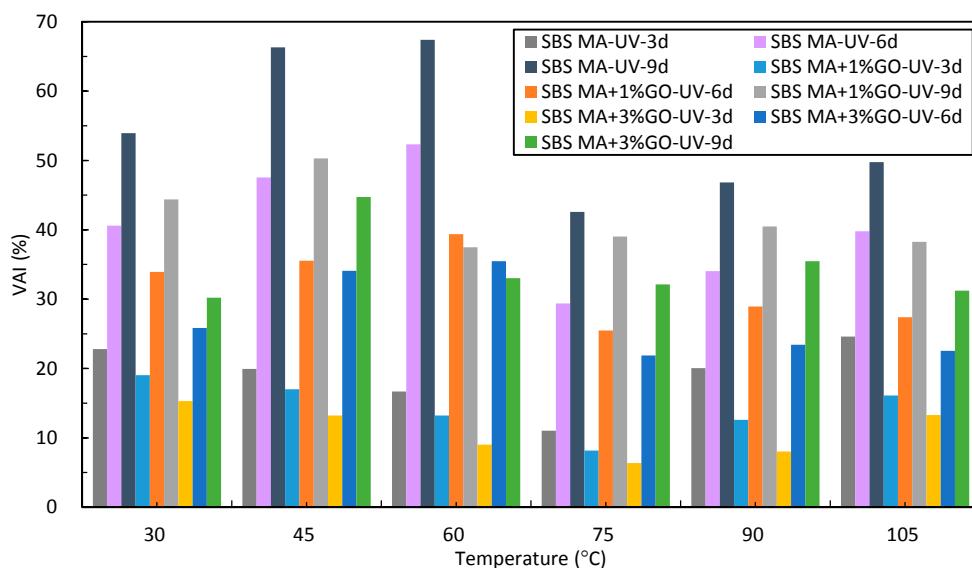
Figure 8. VAI of SBS MA and GO modified SBS MA after UV aging.

The results shown in Figure 7 indicate that the VAI values of all temperatures increase with the increase of the UV-aging time, which shows that the UV-aging degree is increased. For example, the VAI of the GO-modified 90 A decreased as the content of the GO increase. Therefore, for the 90 A binder tested, one can conclude that the GO can improve the UV aging resistance performance and, at the same UV-aging condition, the VAI of the 1% GO-modified 90 A has no significant difference with 3% GO-modified 90 A. However, the VAI value after adding 3% GO was slightly lower than that of 1% GO.

The VAI results of SBS MA in Figure 8 show the same trend as of 90 A, the VAI is increasing with an increase in UV-aging time. However, the VAI of the GO-modified SBS MA is much smaller than that of SBS MA. It is clear that the GO can improve the UV aging resistance performance of 90 A and

SBS MA, and the UV aging resistance performance will be enhanced by increasing the GO content from 1% to 3%.

3.2.3. Evaluating the Rheological Properties

The complex modulus (G*) and the phase angle (δ) of the 90 A and the GO-modified 90 A before aging and after TFOT aging are shown in Figure 9. In general, a nano-material powder always brings a hardening effect to the asphalt, and G* always increases.

From Figure 9, before aging, the G* increment of 90 A with 1% GO content is minimal, and the G* value of the 3% GO-modified 90 A is slightly lower than 90 A. This is possible due to the softening effect of the CO_2 sealed in the asphalt [33,34]. The δ value of the GO-modified 90 A is lower than the δ of 90 A, the difference is more notable from −10 °C to 0 °C. After TFOT, the ranking order of the G* of 90 A is 1% GO-modified 90 A < 3% GO-modified 90 A < 90 A, and there is little difference of the δ of 90 A and the GO-modified 90 A; the G* increment of the 3% GO-modified 90 A is almost the same as 90 A, but the δ reduction of 3% GO-modified 90 A is less than 90 A. This indicates that 3% GO can improve the thermo-oxidative aging resistance performance of 90 A; when the GO content is 1%, the G* is much smaller than that of 90 A. In addition, the δ reduction is also less than 90 A, so that 1% GO can obviously improve the thermo-oxidative aging resistance performance of 90 A. On the improvement in the thermo-oxidative aging resistance performance of 90 A, the 3% GO-modified effect is not as good as the 1% GO. This could be attributed to the residual CO_2 in the asphalt; the CO_2 will be released at the temperature of 163 °C during TFOT. The release process is equivalent to a stirring action and the asphalt film near the CO_2 bubble is very thin, which can, more or less, speed up the TFOT aging rate and weakens the improvement effect of the GO. In this paper, we simply name the process of releasing CO_2 as stirring and film action. When the GO content is 1%, this stirring and film action is less obvious than with the 3% GO content; hence, a better anti-aging performance.
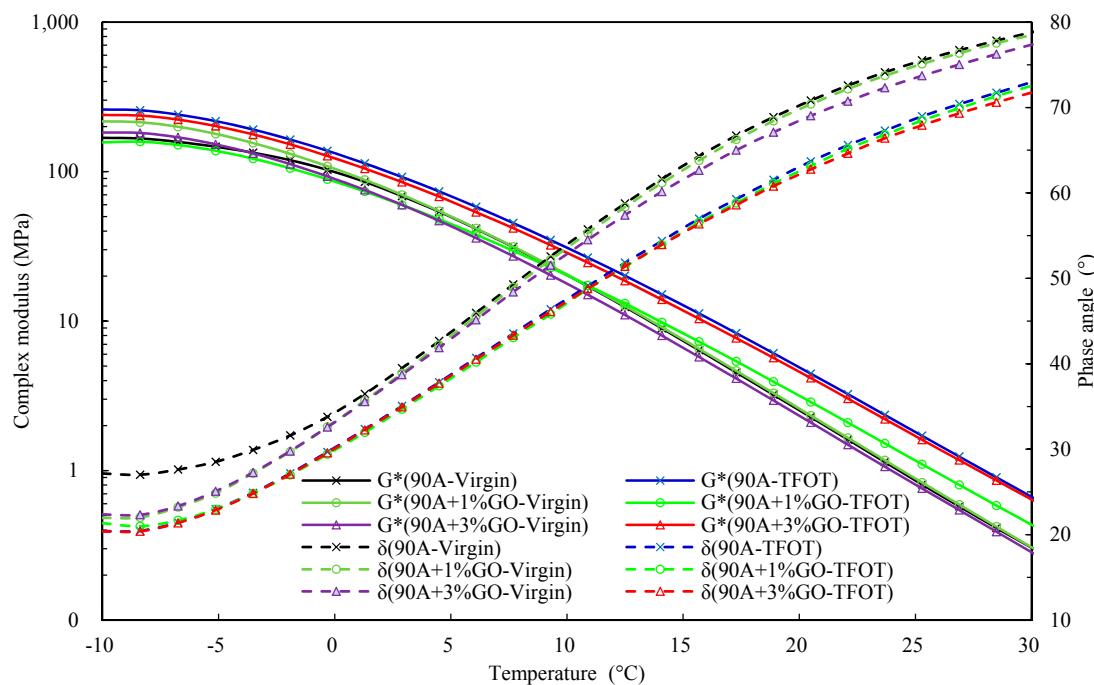
Figure 9. Complex modulus of 90 A and GO modified 90 A before and after TFOT.

The G* and the δ of 90 A and the GO-modified 90 A after TFOT and after nine days of UV aging are shown in Figure 10. After nine days of UV aging, the order of the G* of 90 A was found to be 3% GO-modified 90 A < 1% GO-modified 90 A < 90 A. The G* value is decreased by the utilization of the GO, especially the G* of the 3% GO-modified asphalt after nine days of UV aging is almost the

same as before aging, which shows the GO has an excellent UV aging resistance performance. The GO can significantly improve the anti-UV aging performance of 90 A, and the improvement effect of the 3% GO is much better than 1% GO. The UV test temperature (50 °C) is only slightly higher than its softening point; on the other hand, after 5 h of TFOT aging, CO_2 is released completely out of the GO-modified asphalt, so the stirring and film action will not affect the improvement effect of the GO.
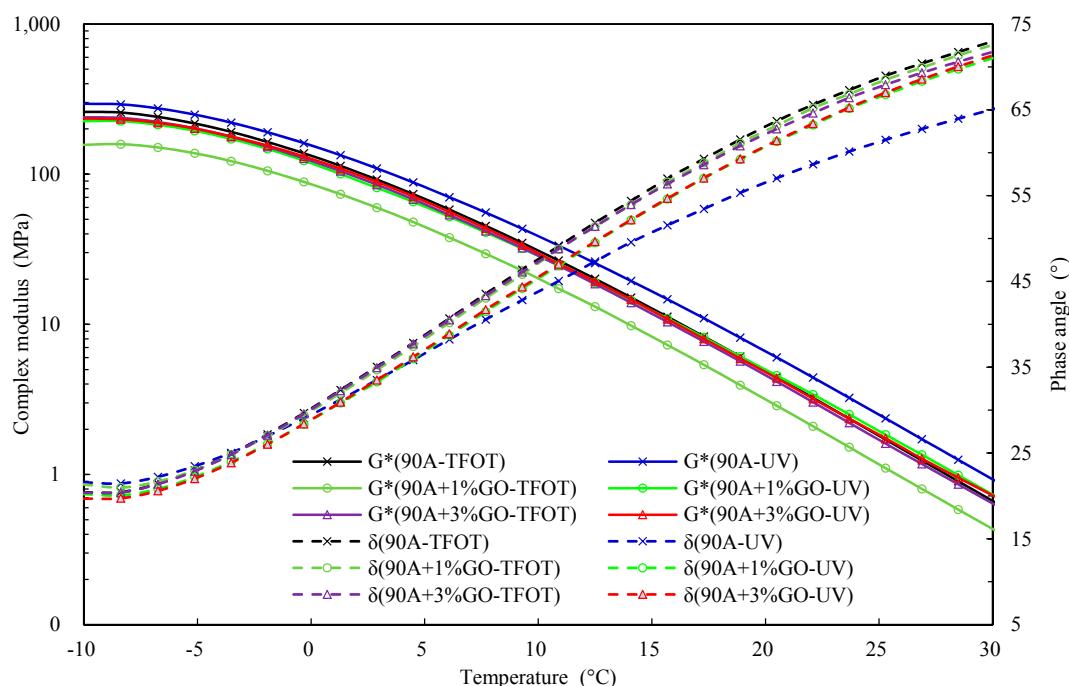
Figure 10. Complex modulus of 90 A and GO modified 90 A after TFOT and nine days of UV aging.

The fatigue cracking factor (G*sinδ) is used to evaluate the anti-fatigue performance of an asphalt binder where the lower value of the G*sinδ is an indication of better anti-fatigue performance. Superpave specifications specify that the G*sinδ should not be higher than 5.0 MPa [35]. In this paper, in order to quantitatively evaluate the effects of the GO on the anti-fatigue performance of asphalt at different aging states, the corresponding temperature fatigue cracking factor of 5.0 MPa is also calculated; this temperature is simply referred to as FFT.

Figure 11 shows the G*sinδ results of 90 A and the GO-modified 90 A. It can be found from this figure that the order of G*sinδ after UV aging is 3% GO-modified 90 A < 1% GO-modified 90 A < 90 A, indicating that the GO can improve the anti-fatigue performance of 90 A after UV aging, and the improvement effect of 3% GO is much better than 1% GO.

Table 2 shows the FFT of 90 A and SBS MA. It can be observed from Table 2 that, before aging, the FFT of the 1% GO-modified 90 A is the same as the 90 A, and the FFT of the 3% GO-modified 90 A is 0.7 °C lower than 90 A, so the GO can slightly improve the anti-fatigue performance of 90 A before aging. After TFOT, the FFT of 90 A and the GO-modified 90 A all increased, but the FFT of the 1% and 3% GO-modified 90 A were 2.6 °C and 0.5 °C lower than 90 A. This trend was the same for the G and δ values. After UV aging, the order of the TTF was found to be 3% GO-modified 90 A < 1% GO-modified 90 A < 90 A. The change above proves that GO can improve the anti-aging performance of an asphalt binder, the fatigue cracking resistance performance of the GO-modified 90 A are better than 90 A at any aging states, and the improvement effect will be more significant after aging.
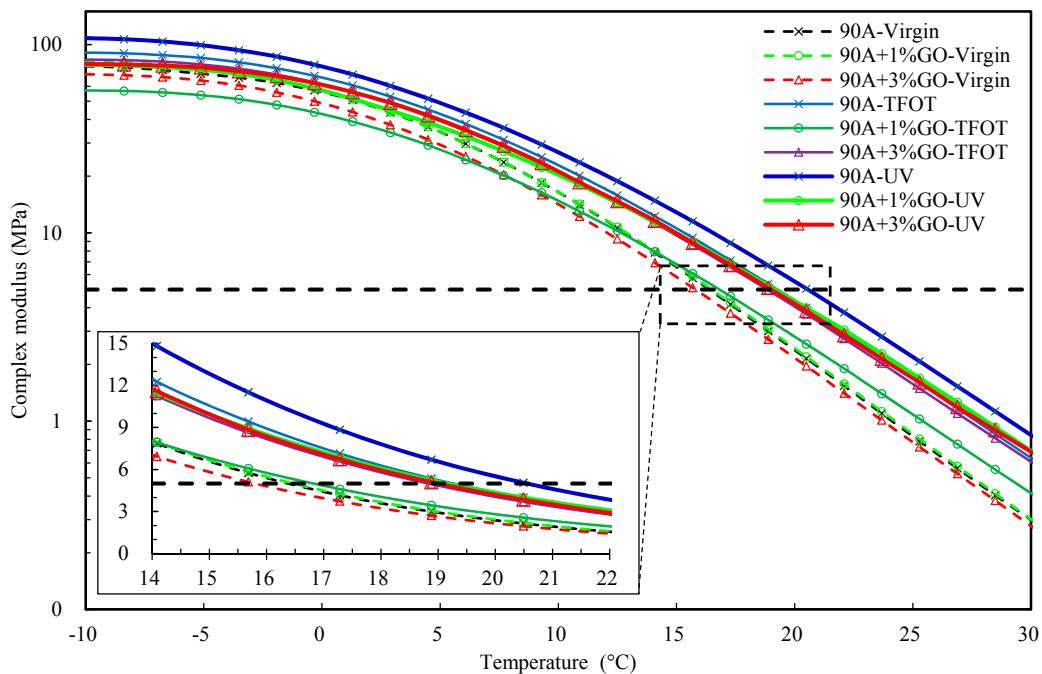
Figure 11. Fatigue cracking factor of 90 A and GO-modified 90 A.

Table 2. The FFT of 90 A and GO-modified 90 A.

Aging Degree	Virgin			TFOT Aging			UV Aging		
GO content (%)	0	1	3	0	1	3	0	1	3
FFT (°C)	16.5	16.5	15.8	19.3	16.7	18.8	20.6	19.2	19.0

The G* and the δ of SBS MA and the GO-modified SBS MA before aging and after TFOT are shown in Figure 12. Before aging, the GO did not increase the G* of the SBS MA significantly, the G* curve of GO-modified SBS MA almost overlap with the SBS MA without the GO. With the increase of GO content, the δ of the SBS MA only slightly decreases. The slight changes of the G* and the δ show the GO will not obviously decrease the low-temperature performance of the SBS MA. After TFOT aging, the G* increases while the δ decreases, which shows the increment of the asphalt aging degree. Compared to SBS MA, the G* increment and the δ decrement of the GO-modified SBS MA is almost the same, so the GO is not able to improve the thermo-oxidative aging resistance performance of SBS MA significantly. The improvement effect of the GO during TFOT may be weakened by the stirring and film action of the CO_2, and the viscosity of the SBS MA increase more sharply than the 90 A with the decrease of the temperature, which may seal more CO_2 in the asphalt. The CO_2 sealed in the asphalt will be released when the viscosity decreases at high temperature during TFOT. Thus, there is no obvious improvement of the SBS MA anti-TFOT aging performance.

The G* and the δ of SBS MA and the GO-modified SBS MA after TFOT and after nine days of UV aging are shown in Figure 13. After UV aging, the order of the G* is 3% GO-modified SBS MA < 1% GO modified SBS MA < SBS MA, and the G* increment of 3% GO-modified SBS MA is the lowest, 1% GO modified SBS MA is the second and SBS MA is the largest, there is no obvious difference of the δ of these three kinds of SBS MA binders. Thus, the order of the anti-UV aging performance is 3% GO-modified SBS MA > 1% GO-modified SBS MA > SBS MA. Therefore, one can conclude that, for these binders, GO can improve the anti-UV aging performance of SBS MA and the improvement of the 3% GO is better than that of the 1% GO.
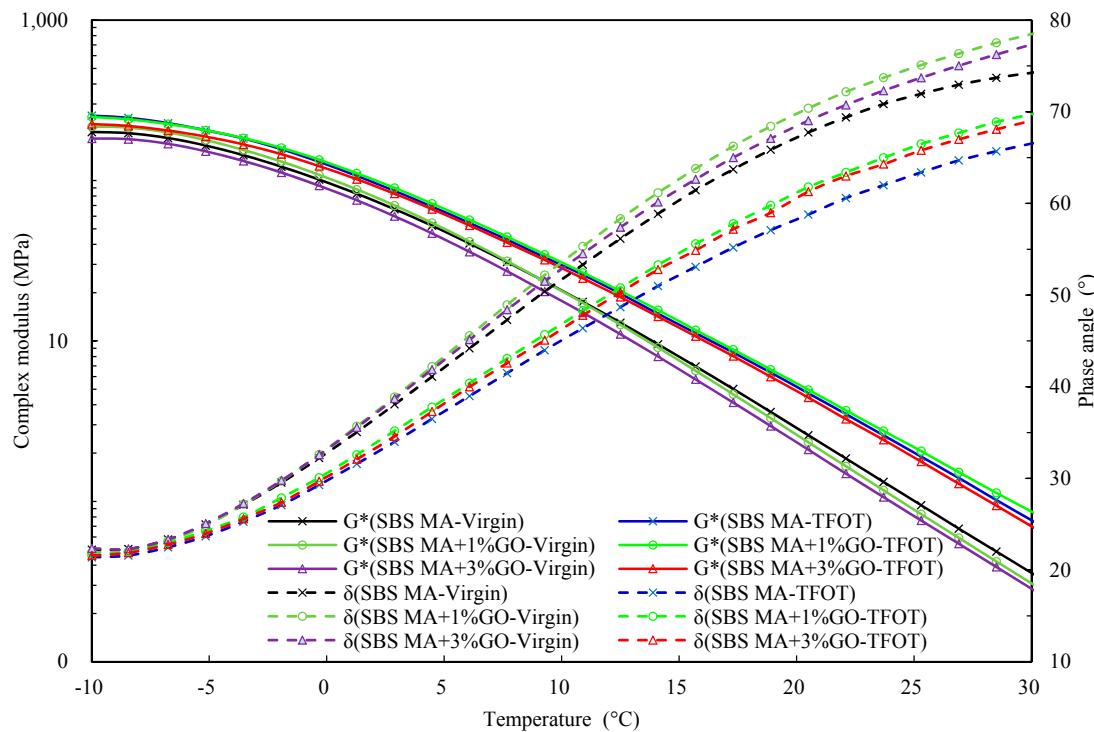
Figure 12. Complex modulus of SBS MA and GO modified SBS MA before and after TFOT.
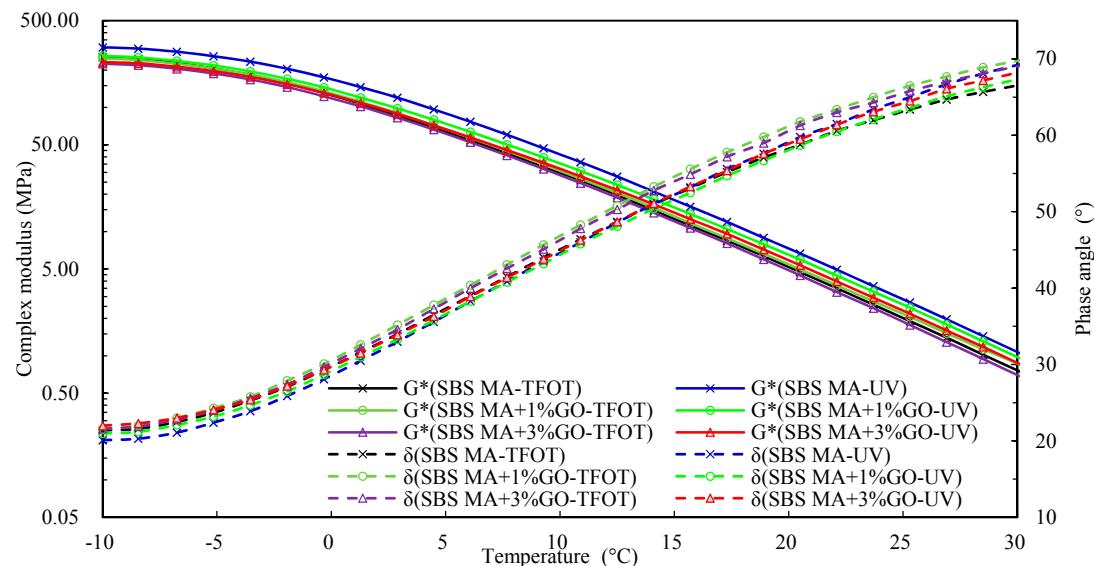
Figure 13. Complex modulus of SBS MA and GO-modified SBS MA after TFOT and nine days UV aging.

The G*sinδ of SBS MA and GO-modified SBS MA after UV aging are shown in Figure 14. With the increment of the GO content, the G*sinδ decreases, which shows that the fatigue property is improved after adding the GO, and the results of the 3% GO content is better than 1% GO content.

Table 3 gives the FFT results of SBS MA and the GO-modified SBS MA. Before aging, the FFT order of SBS MA is almost the same as 90 A, the1% GO and the 3% GO modified SBS MA are 0.2 °C and 1.0 °C smaller than SBS MA. Therefore, the GO can improve the fatigue cracking resistance performance of the SBS MA before aging. After TFOT, the FFT of the 3% GO-modified SBS MA are lower than the SBS MA; the FFT of the 1% GO-modified SBS MA are higher than SBS MA, but the

increment is only 0.7 °C, which will not greatly reduce the low-temperature performance of a binder. Thus, 3% GO can slightly improve the anti-TFOT aging of SBS MA, while 1% GO slightly decreases the anti-TFOT aging of SBS MA. After UV aging, the order of the TTF is 3% GO-modified SBS MA < 1% GO SBS MA < SBS MA, the1% GO and the 3% GO-modified SBS MA are 0.8 °C and 1.3 °C lower than SBS MA. Fatigue cracking resistance performances of the modified SBS MA are better than 90 A after UV aging. Therefore, one can conclude that GO can improve the UV aging resistance performance of SBS MA, and the improvement effect of the 3% GO is better than the 1% GO.
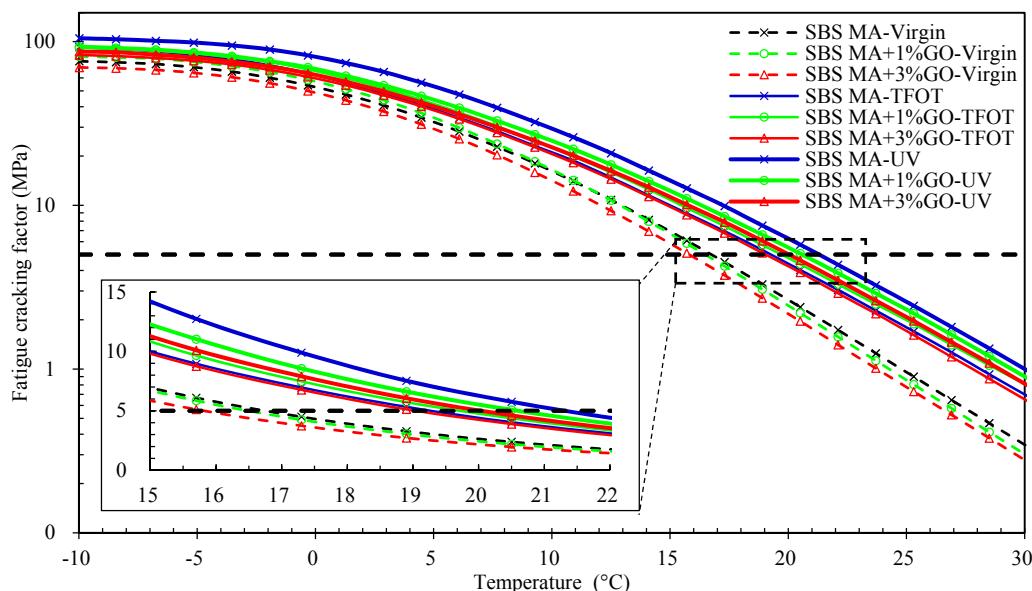
Figure 14. Fatigue cracking factor of SBS MA and GO-modified SBS MA.

Table 3. The FFT of the SBS MA and GO-modified SBS MA.

Aging Degree	Virgin			TFOT Aging			UV Aging		
GO content (%)	0	1	3	0	1	3	0	1	3
FFT (°C)	16.8	16.6	15.8	19.3	19.8	19.1	21.4	20.6	20.1

4. Conclusions

The $I_{C=O}$ and $I_{S=O}$ before and after UV aging were tested by the FTIR to study the chemical structure changes of the GO-modified asphalt during UV aging. The PRR, SPI, DRR, and the VAI were calculated and analyzed to estimate the physical properties changes of the GO-modified asphalt during UV aging. Finally, the DSR was used to study the rheological properties, G^* and δ, before and after aging. After analyzing the results of these tests, the following conclusions can be made:

1. Before aging, the GO could decrease the G^* and slightly change the δ of 90 A and SBS MA; in total, a smaller $G^*\sin\delta$ value was obtained after being modified by the GO, which shows that the GO could improve the fatigue cracking resistance performance of the 90 A and SBS MA binders.
2. According to the rheological property testing, before and after TFOT, the GO could improve the thermo-oxidative aging resistance performance of 90 A and SBS MA, and the improvement effect of the GO on 90 A was better than SBS MA.
3. After UV aging, the $I_{C=O}$ and $I_{S=O}$ increment of the GO modified asphalt were smaller than that of the asphalt without GO. The GO could retard the formations of the carbonyl and sulfoxide groups during UV aging, and decrease the aging degree of 90 A and SBS MA.
4. After UV aging, the GO could increase the PRR and DRR of 90 A and SBS MA, meanwhile decreasing the SPI and VAI; the order of the G^* was 3% GO-modified asphalt < 1% GO-modified

asphalt < 90 A (or SBS MA). The increment of G* was obviously decreased after adding the GO, and the fatigue cracking resistance performance of GO-modified asphalt were better than that of the asphalt without the GO. The results showed that the GO could improve the stability of the asphalt physical performance. The GO could improve the UV aging resistance performance of 90 A and SBS MA obviously, and the improvement effect of the 3% GO was better than that of 1% GO.

Author Contributions: Shaopeng Wu, Zhijie Zhao, and Ling Pang conceived and designed the experiments. Zhijie Zhao, Yuanyuan Li, and Martin Riara performed the experiments. Shaopeng Wu, Ling Pang, Serji Amirkhanian, and Zhijie Zhao analyzed the data. Yuanyuan Li and Martin Riara contributed reagents/materials/analysis tools. Shaopeng Wu, Zhijie Zhao, Ling Pang, and Yuanyuan Li wrote the paper. Martin Riara and Ling Pang designed the software used in analysis. Serji Amirkhanian reviewed the paper.

Conflicts of Interest: The authors declare no conflict of interest.

References

1. Rasool, R.T.; Wang, S.; Zhang, Y.; Li, Y.; Zhang, G. Improving the aging resistance of SBS modified asphalt with the addition of highly reclaimed rubber. *Constr. Build. Mater.* **2017**, *145*, 126–134. [CrossRef]

2. Behnood, A.; Olek, J. Rheological Properties of asphalt binders modified with styrene-butadiene-styrene (SBS), ground tire rubber (GTR), or polyphosphoric acid (PPA). *Constr. Build. Mater.* **2017**, *151*, 464–478. [CrossRef]

3. Islam, M.R.; Tarefder, R.A. Study of asphalt aging through beam fatigue test. *Transp. Res. Rec. J. Transp. Res. Board* **2015**, *2505*, 115–120. [CrossRef]

4. Pang, L.; Liu, K.; Wu, S.; Lei, M.; Chen, Z. Effect of LDHs on the aging resistance of crumb rubber modified asphalt. *Constr. Build. Mater.* **2014**, *67*, 239–243. [CrossRef]

5. Apeagyei, A.K. Laboratory evaluation of antioxidants for asphalt binders. *Constr. Build. Mater.* **2011**, *25*, 47–53. [CrossRef]

6. Petersen, J.C. A review of the fundamentals of asphalt oxidation: Chemical, physicochemical, physical property and durability relationships. Transportation research circular e-c140. *Transp. Res. E-Circ.* **2009**. [CrossRef]

7. Feng, Z.G.; Wang, S.J.; Bian, H.J.; Guo, Q.L.; Li, X.J. FTIR and rheology analysis of aging on different ultraviolet absorber modified bitumens. *Constr. Build. Mater.* **2016**, *115*, 48–53. [CrossRef]

8. Zhang, C.; Yu, J.; Xue, L.; Sun, Y. Investigation of γ-(2,3-Epoxypropoxy) propyltrimethoxy Silane Surface Modified Layered Double Hydroxides Improving UV Ageing Resistance of Asphalt. *Materials* **2017**, *10*, 78. [CrossRef]

9. Yu, J.Y.; Feng, P.C.; Zhang, H.L.; Wu, S.P. Effect of organo-montmorillonite on aging properties of asphalt. *Constr. Build. Mater.* **2009**, *23*, 2636–2640. [CrossRef]

10. Zhang, H.; Yu, J.; Wu, S. Effect of montmorillonite organic modification on ultraviolet aging properties of SBS modified bitumen. *Constr. Build. Mater.* **2012**, *27*, 553–559. [CrossRef]

11. Cong, P.; Xu, P.; Chen, S. Effects of carbon black on the anti aging, rheological and conductive properties of SBS/asphalt/carbon black composites. *Constr. Build. Mater.* **2014**, *52*, 306–313. [CrossRef]

12. Feng, Z.; Yu, J.; Wu, S. Rheological evaluation of bitumen containing different ultraviolet absorbers. *Constr. Build. Mater.* **2012**, *29*, 591–596. [CrossRef]

13. Nazari, M.H.; Shi, X. Polymer-Based Nanocomposite Coatings for Anticorrosion Applications. In *Industrial Applications for Intelligent Polymers and Coatings*; Springer International Publishing: New York, NY, USA, 2016.

14. Park, S.; Lee, K.S.; Bozoklu, G.; Cai, W.; Nguyen, S.T.; Ruoff, R.S. Graphene oxide papers modified by divalent ions—Enhancing mechanical properties via chemical cross-linking. *ACS Nano* **2008**, *2*, 572–578. [CrossRef] [PubMed]

15. Wang, L.; Wang, D.; Dong, X.Y.; Zhang, Z.J.; Pei, X.F.; Chen, X.J.; Chen, B.; Jin, J. Layered assembly of graphene oxide and Co–Al layered double hydroxide nanosheets as electrode materials for supercapacitors. *Chem. Commun.* **2011**, *47*, 3556–3558. [CrossRef] [PubMed]

16. Tang, Z.; Wu, X.; Guo, B.; Zhang, L.; Jia, D. Preparation of butadiene–styrene–vinyl pyridine rubber–graphene oxide hybrids through co-coagulation process and in situ interface tailoring. *J. Mater. Chem.* **2012**, *22*, 7492–7501. [CrossRef]

17. ASTM D5/D5M. *Standard Test Method for Penetration of Bituminous Materials*; American Society for Testing and Materials: West Conshohocken, PA, USA, 2013.

18. ASTM D36/D36M. *Standard Test Method for Softening Point of Bitumen (Ring and Ball Apparatus)*; American Society for Testing and Materials: West Conshohocken, PA, USA, 2012.

19. ASTM D113. *Standard Test Method for Ductility of Bituminous Materials*; American Society for Testing and Materials: West Conshohocken, PA, USA, 2007.

20. ASTM D4402. *Standard Test Method for Viscosity Determination of Asphalt at Elevated Temperatures Using a Rotational Viscometer*; American Society for Testing and Materials: West Conshohocken, PA, USA, 2013.

21. Yoo, B.M.; Shin, H.J.; Yoon, H.W.; Park, H.B. Graphene and graphene oxide and their uses in barrier polymers. *J. Appl. Polym. Sci.* **2014**, *131*. [CrossRef]

22. Lerf, A.; He, H.; Forster, M.; Klinowski, J. Structure of graphite oxide revisited. *J. Phys. Chem. B* **1998**, *102*, 4477–4482. [CrossRef]

23. He, H.; Klinowski, J.; Forster, M.; Lerf, A. A new structural model for graphite oxide. *Chem. Phys. Lett.* **1998**, *287*, 53–56. [CrossRef]

24. Eda, G.; Chhowalla, M. Chemically derived graphene oxide: Towards large-area thin-film electronics and optoelectronics. *Adv. Mater.* **2010**, *22*, 2392–2415. [CrossRef] [PubMed]

25. Kim, J.; Cote, L.J.; Kim, F.; Yuan, W.; Shull, K.R.; Huang, J. Graphene oxide sheets at interfaces. *J. Am. Chem. Soc.* **2010**, *132*, 8180–8186. [CrossRef] [PubMed]

26. Li, X.; Zhang, G.; Bai, X.; Sun, X.; Wang, X.; Wang, E.; Dai, H. Highly conducting graphene sheets and Langmuir–Blodgett films. *Nat. Nanotechnol.* **2008**, *3*, 538–542. [CrossRef] [PubMed]

27. Kudin, K.N.; Ozbas, B.; Schniepp, H.C.; Prud'Homme, R.K.; Aksay, I.A.; Car, R. Raman spectra of graphite oxide and functionalized graphene sheets. *Nano Lett.* **2008**, *8*, 36–41. [CrossRef] [PubMed]

28. Sun, P.; Zhu, M.; Wang, K.; Zhong, M.; Wei, J.; Wu, D.; Xu, Z.; Zhu, H. Selective ion penetration of graphene oxide membranes. *ACS Nano* **2012**, *7*, 428–437. [CrossRef] [PubMed]

29. Yu, L.; Lim, Y.S.; Han, J.H.; Kim, K.; Kim, J.Y.; Choi, S.Y.; Shin, K. A graphene oxide oxygen barrier film deposited via a self-assembly coating method. *Synth. Met.* **2012**, *162*, 710–714. [CrossRef]

30. Usuki, A.; Kojima, Y.; Kawasumi, M.; Okada, A.; Fukushima, Y.; Kurauchi, T.; Kamigaito, O. Synthesis of nylon 6-clay hybrid. *J. Mater. Res.* **1993**, *8*, 1179–1184. [CrossRef]

31. Priolo, M.A.; Gamboa, D.; Holder, K.M.; Grunlan, J.C. Super gas barrier of transparent polymer−clay multilayer ultrathin films. *Nano Lett.* **2010**, *10*, 4970–4974. [CrossRef] [PubMed]

32. LeBaron, P.C.; Wang, Z.; Pinnavaia, T.J. Polymer-layered silicate nanocomposites: An overview. *Appl. Clay Sci.* **1999**, *15*, 11–29. [CrossRef]

33. Zeng, W.; Wu, S.; Pang, L.; Sun, Y.; Chen, Z. The utilization of graphene oxide in traditional construction materials: Asphalt. *Materials* **2017**, *10*, 48. [CrossRef]

34. Schniepp, H.C.; Li, J.L.; McAllister, M.J.; Sai, H.; Herrera-Alonso, M.; Adamson, D.H.; Prud'homme, R.K.; Car, R.; Saville, D.A.; Aksay, I.A. Functionalized single graphene sheets derived from splitting graphite oxide. *J. Phys. Chem. B* **2006**, *110*, 8535–8539. [CrossRef] [PubMed]

35. AASHTO T315. *Determining the Rheological Properties of Asphalt Binder Using a Dynamic Shear Rheometer*; American Association of State Highway and Transportation Officials: Washington, DC, USA, 2010.